Journal of Hydraulic Research
Publication details, including instructions for authors and subscription information:
http://www.tandfonline.com/loi/tjhr20

Optimization of ADV sampling strategies using DNS of turbulent flow

Vicente G. Gil Montero[a], Martín Romagnoli[b], Carlos M. García[c], Mariano I. Cantero[d] & Graciela Scacchi[e]

[a] PhD Student, División de Mecánica Computacional, Centro Atómico Bariloche, Comisión Nacional de Energía Atómica (CNEA), Bariloche, Argentina

[b] Research Fellow, Centro Internacional Franco Argentino de Ciencias de la Información y de Sistemas (CIFASIS - CONICET - UNR - AMU) / Centro Universitario Rosario de Investigaciones Hidroambientales (CURIHAM - UNR). Ocampo y Esmeralda, S2000EZP, Rosario, Argentina

[c] Associated Professor, Consejo Nacional de Investigaciones Científicas y Técnicas (CONICET), Centro de Estudios y Tecnología del Agua (CETA - UNC), Córdoba, Argentina

[d] Associated Professor, Consejo Nacional de Investigaciones Científicas y Técnicas (CONICET), División de Mecánica Computacional, Centro Atómico Bariloche, Comisión Nacional de Energía Atómica (CNEA) / Instituto Balseiro (IB - CNEA - UNC), Bariloche, Argentina

[e] Facultad de Ingeniería y Ciencias Hídricas (FICH - UNL), Santa Fe, Argentina

Published online: 21 Nov 2014.

To cite this article: Vicente G. Gil Montero, Martín Romagnoli, Carlos M. García, Mariano I. Cantero & Graciela Scacchi (2014): Optimization of ADV sampling strategies using DNS of turbulent flow, Journal of Hydraulic Research, DOI: 10.1080/00221686.2014.967818

To link to this article: http://dx.doi.org/10.1080/00221686.2014.967818

IAHR AIRH
Taylor & Francis
Taylor & Francis Group

Journal of Hydraulic Research, 2014
http://dx.doi.org/10.1080/00221686.2014.967818

Technical note

Optimization of ADV sampling strategies using DNS of turbulent flow

VICENTE G. GIL MONTERO, PhD Student, *División de Mecánica Computacional, Centro Atómico Bariloche, Comisión Nacional de Energía Atómica (CNEA), Bariloche, Argentina*

MARTÍN ROMAGNOLI, Research Fellow, *Centro Internacional Franco Argentino de Ciencias de la Información y de Sistemas (CIFASIS – CONICET – UNR – AMU) / Centro Universitario Rosario de Investigaciones Hidroambientales (CURIHAM – UNR). Ocampo y Esmeralda, S2000EZP, Rosario, Argentina*
Email: romagnoli@cifasis-conicet.gov.ar (author for correspondence)

CARLOS M. GARCÍA, Associated Professor, *Consejo Nacional de Investigaciones Científicas y Técnicas (CONICET), Centro de Estudios y Tecnología del Agua (CETA – UNC), Córdoba, Argentina*

MARIANO I. CANTERO, Associated Professor, *Consejo Nacional de Investigaciones Científicas y Técnicas (CONICET), División de Mecánica Computacional, Centro Atómico Bariloche, Comisión Nacional de Energía Atómica (CNEA) / Instituto Balseiro (IB – CNEA – UNC), Bariloche, Argentina*

GRACIELA SCACCHI, Associated Professor, *Facultad de Ingeniería y Ciencias Hídricas (FICH – UNL), Santa Fe, Argentina*

ABSTRACT
This work presents an investigation on the effects of spatial and temporal averaging processes (filtering) implemented in an Acoustic Doppler Velocimeter (ADV) on the computations of the turbulent kinetic energy, velocity variances, and Reynolds shear stresses. The averaging processes are implemented in the ADV technology in order to reduce the noise level inherent in acoustic measurements. A conceptual model, simulating the ADV operation and the turbulent flow field, is developed to assess the filtering effects on the turbulence parameter estimates of sampling volume heights, recording frequencies, and distances from the sampling volume to the channel bottom. The results of the conceptual model are compared with experimental data. The findings provide a criterion to examine the capability of ADV to characterize turbulent flows using different sampling configurations.

Keywords: Acoustic Doppler velocimeter, direct numerical simulation, sampling strategy

1 Introduction

Acoustic Doppler velocimeters (ADVs) are capable of reporting accurate mean values of water velocity in three dimensions (Kraus, Lohrmann, & Cabrera, 1994, López & Garcia, 2001), even at low velocities (Lohrmann, Cabrera, & Kraus, 1994). However, the use of ADVs to characterize turbulent flows requires assessment of some important aspects such as noise presence (spikes and Doppler noise) and filtering effects due to the sampling strategy implemented by ADVs (spatial and temporal averaging processes) in order to reduce the noise levels (García, Cantero, Niño, & García, 2005; Goring & Nikora, 2002; Romagnoli, García, & Lopardo, 2012; Voulgaris & Trowbridge, 1998). Most recent research exploring ADV capabilities to measure flow turbulence (specifically turbulent kinetic energy and the power spectrum) has been focused on noise presence and how it can be reduced or removed (Blanckaert & Lemmin, 2006; [5, Doroudian, Bagherimiyab, & Lemmin, 2010]; Goring & Nikora, 2002; Nikora & Goring, 1998; McLelland & Nicholas, 2000; Parsheh, Sotiropoulos, & Porté-Agel, 2010). On the other hand, little attention has been devoted to evaluate filtering effects due to the sampling strategy implemented in ADV on the turbulence statistics computed from the recorded signals.

García et al. (2005) analysed the effects of the temporal averaging process on the main turbulence parameters computed for the streamwise direction. They reported that an ADV produces a reduction in the moments of the water velocity signals due to the fact that the temporal averaging process acts as a low-pass filter. Additionally, the temporal averaging process affects the autocorrelation functions increasing autocorrelation values for small

Received 27 August 2013; accepted 21 August 2014/Currently open for discussion

ISSN 0022-1686 print/ISSN 1814-2079 online
http://www.tandfonline.com

lag times, producing biased estimates of the time scales computed from autocorrelation, and leading to a reduced resolution of the inertial range of the power spectrum.

This work extends the study of García et al. (2005) by incorporating spatial and temporal averaging processes in the analysis. A conceptual model, simulating the flow field with Direct Numerical Simulation (DNS) and sampling with ADV operation strategy, is developed to assess the effects of spatial and temporal averaging processes (filtering) implemented in ADV on the computations of the turbulent kinetic energy, velocity variances (in the streamwise, spanwise and vertical direction), and Reynolds shear stresses.

2 Principle of operation

An ADV measures all three components of the velocity vector using a pulse-coherent technique (Lhermitte & Serafin 1984). It includes a sound emitter, three or four sound receivers, and a signal conditioning electronic module (SonTek, 2001). Basically, the instrument emits a pair of pulses of duration Δt a short time apart ($\Delta\tau \gg \Delta t$) and measures the phase shift between the reflected signals. If the along-beam water velocity is v_b, the backscattering particles in the water travel along-beam distance $v_b\Delta\tau$ during the interval $\Delta\tau$. Therefore, the travel time difference between two reflected pulses is $2v_b\Delta\tau/c$ where c is the speed of the sound in water, which means that the phase shift $\Delta\varphi$ between the two backscattered pulses is $2\pi f_o(2v_b\Delta\tau/c)$. Here f_o is the ADV acoustic frequency. The instrument measures this phase shift $\Delta\varphi$ to determine the along-beam water velocity as:

$$v_b = c\Delta\varphi/(4\pi f_o\Delta\tau) = \lambda\Delta\varphi/(4\pi\Delta\tau) \quad (1)$$

where $\lambda = c/f_o$ is the wavelength. The phase shift is computed using the covariance method (Miller & Rochwarger, 1972; Zrnic, 1977). One inherent consequence of the pulse-coherent technique is the ambiguous determination of the phase shift (i.e., phase wrapping occurs if the actual phase shift is outside $-\pi < \Delta\varphi < \pi$). The ADV technology uses a dual pulse-pair scheme with different lags $\Delta\tau$ separated by a dwell time (McLelland & Nicholas, 2000). The additional shorter pulse-pair is introduced to avoid phase wrapping.

Each transmitter/receiver pair is appropriately aligned defining the beam axes and the sampling volume. The along-beam velocities are converted to the Cartesian velocities by an internal processing module using a calibration matrix. The sampling volume resembles, approximately, a cylinder with the axis along the axis of the transmitter. The transmitter diameter gives the sampling volume diameter (ϕ), while the convolution of the acoustic pulse length with the receive window over which the return signal is sampled defines the sampling volume height (h_v). Typical instruments from Sontek/YSI and Nortek As have the same sampling volume diameter, $\phi = 6$ mm, while the exact sampling volume height depends on the instrument model and manufacturing company.

In the case of SonTek/YSI, the sampling volume height is 4.5 mm for the 16 MHz MicroADV and 9 mm for the 10 MHz ADV. The user can alter the sampling volume height with software modifications. Reducing both the length of the acoustic pulse and the time window over which the return signal is sampled to minimum makes the height of the sampling volume 1.2 mm for 16 MHz MicroADV and 10 MHz ADV. On the other hand, Nortek As allows the users to define the height of the sampling volume between 3 mm and 15 mm for the Vectrino ADV and between 5 mm and 20 mm for the Vector ADV. Although, within the sampling volume, many backscattering particles move, only one velocity vector is reported. This can be thought as some kind of spatial averaging.

After one (quasi) instantaneous velocity vector is determined for the whole sampling volume, the next process performed by the ADV relates to the temporal averaging. Since the instrument employs different frequencies for sampling (f_s) and recording

Table 1 Maximum sampling frequencies f_s for different ADV models currently available. The maximum recording frequencies f_R defined by the user are: 50 Hz for Sontek/YSI MicroADV 16 MHz; 200 Hz for Nortek Lab or Field Vectrino with 'Vectrino Plus' firmware and 25 Hz for the same instrument with the 'standard' firmware; and 64 Hz for Nortek vector

Velocity Maximum sampling frequencies f_s for different ADV models (Hz)				
RangeSontek/YSI		Nortek Vectrino Lab. or Field		Nortek
($m\,s^{-1}$)	Micro ADV16 (MHz)	VectrinoPlus Firmware	Standard Vector Firmware	Vector
7				125
4		2564	641	125
2.5	263	1818	455	125
2				125
1	256	1754	439	125
0.3	226	1124	281	125
0.1	180	667	167	125
0.03	143	426	107	
0.01				70

(f_R) signals, a temporal average of N values is performed in order to reduce the Doppler noise. Thus, $f_R = f_s/N$. This second averaging process is a digital non-recursive temporal filter (Bendat & Piersol, 2000, García et al., 2005). Table 1 reports the time sampling strategies for several ADVs. For the MicroADV Sontek/YSI the maximum sampling frequency ranges between 143 Hz and 263 Hz depending on the flow velocity range. The higher sampling frequency of Vectrino is due to the fact that the MicroADV performs a sequential sampling of each receiver while Vectrino performs a simultaneous sampling for all the receivers.

3 Conceptual model

A conceptual model was developed to evaluate the effects of the spatial and temporal averaging processes implemented in ADV on the estimates of the turbulence parameters. The model consists of two components that simulate: (1) flow field generated from DNS of turbulent open-channel flow (flow model component), and (2) instrument operation based on ADV procedures described in the preceding section (instrument model component).

3.1 *Flow model component*

Data sets of flow velocities were generated from DNS of turbulent open-channel flow. As the DNS solves all the relevant time and length scales present in the flow without requiring a turbulence closure scheme, it provides the high resolution flow field velocity data required for this work. The simulations are conducted for a horizontal channel in which the flow is driven by a uniform mean pressure gradient in the streamwise direction. The dimensionless set of equations that govern the flow is:

$$\partial \boldsymbol{U}/\partial t + \boldsymbol{U}\nabla\boldsymbol{U} = \boldsymbol{G} - \nabla p + \nabla^2\boldsymbol{U}/\mathsf{R}_\tau \tag{2}$$

$$\nabla\boldsymbol{U} = 0 \tag{3}$$

where $\boldsymbol{U} = (u_x, u_y, u_z)$ is the dimensionless velocity vector, p is the dimensionless pressure, and $\boldsymbol{G} = (1, 0, 0)$ is the dimensionless driving force. Dimensionless variables are defined using (a) the shear velocity $u_* = (\tau_w/\rho)^{1/2}$ where τ_w is the bottom wall shear stress and ρ is the fluid density, as the velocity scale; (b) water depth H as the length scale; (c) H/u_* as the time scale; and (d) ρu_*^2 as the pressure scale. The dimensionless number in Eq. 2 is the friction Reynolds number defined as $\mathsf{R}_\tau = u_* H/\nu$, where ν is kinematic viscosity. For this work, the simulated flow has $\mathsf{R}_\tau = 509$. Based on the analysis of DNS results, the ratio $U_x/u_* = 18$ has been computed, giving a bulk Reynolds number of $\mathsf{R} = 9164$ ($\mathsf{R} = U_x H/\nu$, where U_x is the mean streamwise velocity).

The length of the simulated channel (simulation domain) has been chosen as $L_x = 4\pi H$, the width as $L_y = 4/3\pi H$, and the height as $L_z = H$. The grid resolution used is $N_x \times N_y \times N_z = 256 \times 256 \times 129$ (non-uniform grid in the vertical direction being denser near both the channel bottom and the water surface), and the non-linear terms are computed in a grid $3N_x/2 \times 3N_y/2 \times N_z$ in order to prevent aliasing errors. In terms of wall units the grid resolution is $\Delta x^+ = 24.9$, $\Delta y^+ = 8.3$, $\Delta z^+_{\min} = 0.08$ and $\Delta z^+_{\max} = 6.3$. The bottom wall represents a smooth no-slip boundary and the top wall is a free slip wall. The dimensionless boundary conditions employed in the vertical direction are,

$$\boldsymbol{U} = 0 \text{ at } z/H = 0 \tag{4}$$

and

$$\partial u_x/\partial z = \partial u_y/\partial z = u_z = 0 \text{ at } z/H = 1 \tag{5}$$

where z is the distance from the bed. For the other horizontal directions, periodic boundary conditions are employed. The integration time employed in this work is $50H/u_*$ (100,000 time steps) after the flow has achieved a statistically steady state. Details of the numerical scheme implementation and the code validation can be found in Cortese & Balachandar (1995) and Cantero, Lee, & Balachandar (2007). Although it is not included here, DNS results were also compared with widely used experimental results and semi-theoretical relationships for turbulence parameters (Nezu & Nakagawa, 1993; Tarrab, García, Cantero, & Oberg, 2012).

In order to determine flow conditions to be sampled using the instrument model component, a flow depth $H = 0.0641$ m is defined for the analysis. Using this flow depth, the following values are obtained: $u_* = 0.0079\,\mathrm{m\,s^{-1}}$ (assuming $\nu = 1 \times 10^{-6}\,\mathrm{m^2\,s^{-1}}$), mean streamwise flow velocity $U_x = 0.143\,\mathrm{m\,s^{-1}}$, energy slope = 0.0001 and a channel width of 0.134 m. On the basis of these variables, the temporal resolution of the simulated flow field is 4.035×10^{-3} s (frequency equal to 247.8 Hz). The minimum flow depth constraint on the use of ADVs (i.e. the distance between the centre of the sampling volume and the probe tip) is not relevant for our study.

3.2 *Instrument model component*

Time series of each three flow velocity components are extracted from the DNS by the instrument model component simulating the ADV sampling strategy. The velocity vector for each sampling volume is calculated using a uniform distribution for the spatial weighting function:

$$h(x,y,z) = \begin{cases} \dfrac{1}{IJK} & \begin{array}{l} x_c - l_x/2 \le x \le x_c + l_x/2 \\ y_c - l_y/2 \le y \le y_c + l_y/2 \\ z_c - l_z/2 \le z \le z_c + l_z/2 \end{array} \\ 0 & \text{elsewhere} \end{cases} \tag{6}$$

Here, l_x, l_y and l_z are the sampling volume dimensions along the main axes, $l = l_x/\mathrm{d}x$, $J = l_y/\mathrm{d}y$, $K = l_z/\mathrm{d}z$ where $\mathrm{d}x$, $\mathrm{d}y$ and $\mathrm{d}z$ are the DNS grid resolution at location (x_c, y_c, z_c). This assumption about the spatial weighting function does not strongly affect the analysis presented in this paper since Soulsby

(1980) claimed that the signal attenuation is less sensitive to the $h(x,y,z)$ form than to the sampling volume size. Using the weighting function given by Eq. 6 and the digital non-recursive temporal filter mentioned in Section 2, the 'ADV' velocity vector components are computed as:

$$u(x,y,z,t) = \frac{1}{N}\sum_{n=0}^{N-1}\frac{1}{IJK}\sum_{i=0}^{I-1}\sum_{j=0}^{J-1}\sum_{k=0}^{K-1} u_x \left(x+i\mathrm{d}x, y+j\,\mathrm{d}y, z+k\mathrm{d}z, t+\frac{n}{Nf_R}\right)$$

$$v(x,y,z,t) = \frac{1}{N}\sum_{n=0}^{N-1}\frac{1}{IJK}\sum_{i=0}^{I-1}\sum_{j=0}^{J-1}\sum_{k=0}^{K-1} u_y \left(x+i\mathrm{d}x, y+j\,\mathrm{d}y, z+k\mathrm{d}z, t+\frac{n}{Nf_R}\right)$$

$$w(x,y,z,t) = \frac{1}{N}\sum_{n=0}^{N-1}\frac{1}{IJK}\sum_{i=0}^{I-1}\sum_{j=0}^{J-1}\sum_{k=0}^{K-1} u_z \left(x+i\mathrm{d}x, y+j\,\mathrm{d}y, z+k\mathrm{d}z, t+\frac{n}{Nf_R}\right) \quad (7)$$

where f_R is the recording frequency. The simulated ADV velocity field (u,v,w) is thus obtained from the DNS velocity field (u_x,u_y,u_z) through the spatial and temporal averaging processes, i.e. as an outcome of the instrument model component, Eqs. (6) and (7).

Different sampling volume heights (h_v = 0.8, 2.3, 3.9, 5.4, 7.0 and 8.6 mm); recording frequencies (f_R = 247.8, 49.5, 24.7, 9.9 and 4.9 Hz); and distances from the sampling volume to the channel bed (z = 0.009, 0.032 and 0.055 m) are considered in the analysis. Sampling volume diameter ϕ is fixed and equal to 6 mm. After defining the sampling configuration of the instrument model component, a set of synthetic velocity signals is extracted from the DNS. The synthetic signals are analysed in order to compute the corresponding turbulent parameters. Thus, the variation of these parameters with respect to the DNS associated results (with minimum averaging processes on the basis of the advective length scale and the maximum numerical grid resolution) can be assigned to the effects of the ADV sampling strategy.

4 Results

4.1 *Spatial and temporal filtering analysis*

In order to analyse the effects of spatial and temporal averaging on the turbulence parameters estimates, a simple assumption is proposed on the basis that the smallest flow structure sampled by the instrument is given by the characteristic length scale, L_{ADV}. This characteristic length scale is obtained as the maximum among $L = U_c/f_R$, ϕ and h_v, where U_c is the convection velocity of turbulent structures. The first scale is defined by the sampling frequency limitation while two other scales are determined by spatial constraints of the sampling volume. Therefore, the following dimensionless parameter F_{st} can be defined that accounts for spatial and temporal averaging:

$$F_{st} = z/L_{ADV} = z/\max(L,\phi,h_v) \quad (8)$$

Using the conceptual model, the effects of different sampling volume heights (h_v), recording frequencies (f_R), and distances from the bed to the centre of the sampling volume (z) on the estimates of the turbulence parameters are explored below.

Figures 1 to 5 show the percentages of turbulent kinetic energy, Reynolds shear stress and velocity variances in the streamwise, spanwise and vertical direction (k%, $\langle uw\rangle$%, var_x%, var_y% and var_z%, respectively) remaining in the signal after spatial and temporal averaging as a function of the dimensionless parameter F_{st} (Eq. 8).

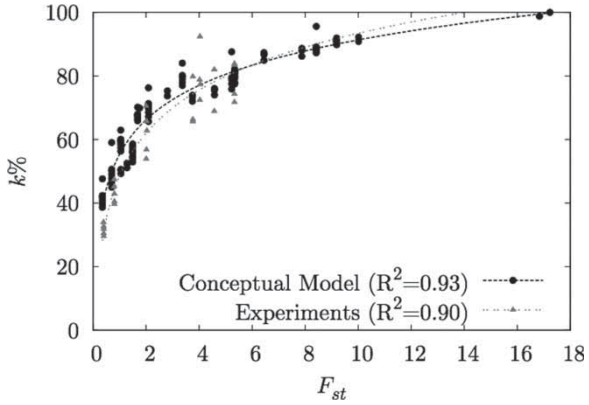

Figure 1 ADV filtering effect on the turbulent kinetic energy estimates evaluated using the conceptual model and the experimental data. k% is the percentage of the energy remaining in the signal after the spatial and time averaging and F_{st} is the dimensionless parameter presented in Eq. 8. Best fit lines for both data sets are also included. R^2 is the squared correlation coefficient of the linearized data

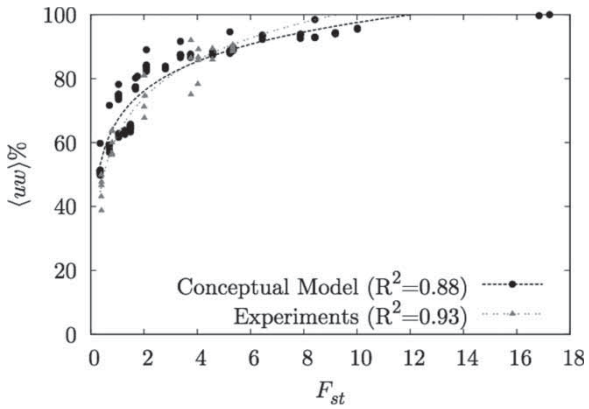

Figure 2 ADV filtering effect on the Reynolds shear stress estimates evaluated using the conceptual model and the experimental data. $\langle uw\rangle$% is the percentage of the Reynolds shear stress remaining in the signal after the spatial and temporal averaging. Best fit lines for both data sets are also included. R^2 is the squared correlation coefficient of the linearized data

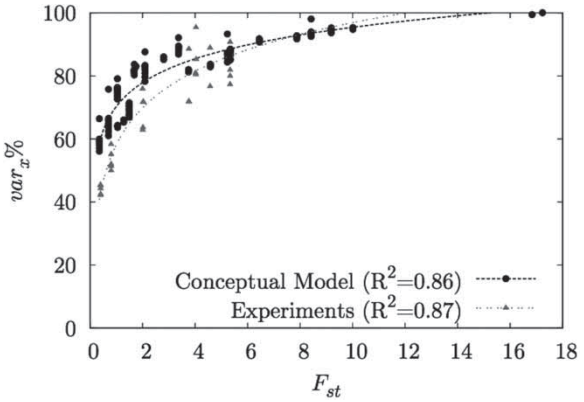

Figure 3 ADV filtering effect on the streamwise velocity variance estimates evaluated using the conceptual model and the experimental data. var_x% is the percentage of the streamwise velocity variance remaining in the signal after the spatial and temporal averaging. Best fit lines for both data sets are also included. R^2 is the squared correlation coefficient of the linearized data

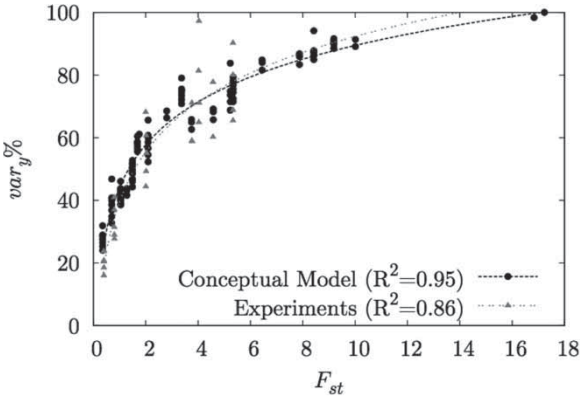

Figure 4 ADV filtering effect on the spanwise velocity variance estimates evaluated using the conceptual model and the experimental data. var_y% is the percentage of the spanwise variance remaining in the signal after the spatial and temporal averaging. Best fit lines for both data sets are also included. R^2 is the squared correlation coefficient of the linearized data

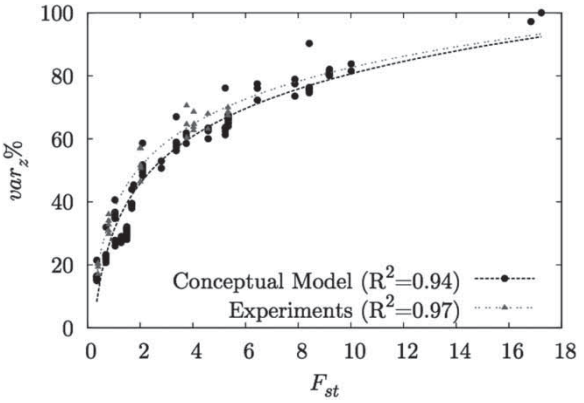

Figure 5 ADV filtering effect on the vertical velocity variance estimates evaluated using the conceptual model and the experimental data. var_z% is the percentage of the vertical variance remaining in the signal after the spatial and temporal averaging. Best fit lines for both data sets are also included. R^2 is the squared correlation coefficient of the linearized data

Table 2 Experimental conditions (Q is flow discharge, H is water depth, U_x is the streamwise mean flow velocity, z is the vertical distance from the sampling volume to the channel bed, $\mathsf{R} = U_x H/\nu$ is the Reynolds number and is the $\mathsf{F} = U_x/\sqrt{Hg}$ is the Froude number)

Q(l s^{-1})	H(m)	U_x (m s^{-1})	z(m)	R	F
12.6	0.08	0.40	0.032	3.2e+04	0.045

The percentages k%, $\langle uw\rangle$%, var_x%, var_y% and var_z% are obtained using ratios k/k_{ref}, $\langle uw\rangle/\langle uw\rangle_{ref}$, var_x/var_{xref}, var_y/var_{yref} and var_z/var_{zref}, where k_{ref}, $\langle uw\rangle_{ref}$, var_{xref}, var_{yref} and var_{zref} are the reference turbulence parameters computed from the velocity signal sampled at the same distance from the channel bed with minimum averaging effects on the basis of both the advective length scale ($L = U_c/f_R$, where $f_R = f_s = 247.8$ Hz) and the maximum numerical grid resolution defining ϕ and h_v (cell sizes are 3.15 mm long, 1.05 mm wide, and $<$0.8 mm high in the vertical direction). First, the percentages k%, $\langle uw\rangle$%, var_x%, var_y% and var_z% are assumed in this work to be equal to 100% at the location with the largest analysed z/L_{ADV} ratio $= F_{st} = 17.23$ (see Figures 1 to 5) in order to define the reference values at this location. Then, at the same location, the effects of different sampling volume heights (h_v) and recording frequencies (f_R), on the estimates of the turbulence parameters were computed and plotted. Using this plot, the reference values for other locations with smaller z values (i.e. smaller z/L_{ADV} ratios) were then estimated. Finally, the effects of different sampling volume heights (h_v) and recording frequencies (f_R), on the estimates of the turbulence parameters were computed at all locations and plotted in Figures 1 to 5.

Figures 1 to 5 show similar trends for the studied parameters, i.e. filtering effects decrease as F_{st} increases and spatial and temporal averaging are most significant for values of F_{st} less than 5. For F_{st} equal to 5 (i.e. flow with convection velocity $U_c = 0.50$ m s^{-1} measured at $z = 0.03$ m with the instrument set to $f_R = 100$ Hz and $h_v = 6$ mm) the percentages k%, $\langle uw\rangle$%, var_x%, var_y% and var_z% remaining in the signal estimated with the conceptual model are 81%, 88%, 88%, 76% and 66%, respectively. The vertical velocity variance is the most affected parameter (var_z% is lower than 20% for $F_{st} = 0.6$ in Fig. 5) because the filtered energy, usually with length scales within the inertial subrange, has a higher relative impact for the vertical component than for the more energy-containing streamwise and spanwise velocity components. On the other hand, the Reynolds shear stress (Fig. 2) and streamwise velocity variance (Fig. 3) are less affected by filtering, both being higher than 65% for $F_{st} = 0.6$.

4.2 *Comparison with experimental data*

The results obtained using the conceptual model are compared with experimental data recorded for this work. The measurements were carried out in a rectangular flume 0.4 m wide, 0.6 m

deep and 16 m long, at the Laboratorio de Hidráulica of Facultad de Ingeniería y Ciencias Hídricas, Universidad Nacional del Litoral, Argentina. The velocity vector time series were recorded using a down-looking 10 MHz Vectrino Nortek with Vectrino Plus firmware. Five different sampling volume heights ($h_v = 2.5$, 4, 5.5,7 and 8.5 mm) and six recording frequencies ($f_R = 200$, 100, 50, 25, 10 and 5 Hz) were employed. The measurements were performed at $z = 0.032$ m from the channel bottom avoiding boundary effects (Precht, Jansse, & Huettel, 2006; Table 2).

The quality of the recorded signals is characterized by a correlation value (COR) ranging from 94 to 98 and a Signal-to-Noise Ratio (SNR) value varying between 39 and 48 dB, which ensure high quality data (Rusello 2009). Most of recorded velocity time series show no spikes. The influence of the Doppler noise was removed following the methodology proposed by Voulgaris & Trowbridge (1998) and verified by Blanckaert & Lemmin (2006). The method computes the noise energy levels for the longitudinal and transversal water velocity components, and averages the energy level in the tail end (noise floor) of each power spectrum. The noise energy level for the vertical velocity component is estimated by averaging the noise levels of the longitudinal and transverse velocity components and dividing the obtained value by a constant calculated from the ADV's calibration matrix. Corrected velocity power spectra were then obtained by subtracting the noise levels from the initial spectra. The corrected variance was then estimated for each flow velocity component as the integral of each corrected power spectra. The variance of velocity signals recorded at $f_R = 200$ Hz, $\phi = 6$ mm, and $h_v = 2.5$ mm and 4 mm, include about a 50% contribution from the measurement noise. Therefore, for the recording frequency $f_R = 200$ Hz, flow velocity signals recorded at $h_v = 2.5$ mm and 4 mm were not used in the present analysis.

The reference values of the turbulence parameters with minimum filtering effects are needed to make the data dimensionless for comparison with the DNS data. The percentages k%, $\langle uw \rangle$%, var_x%, var_y% and var_z% have been obtained using the reference turbulence parameters computed from the velocity signal sampled with the best available sampling configuration ($f_R = 200$ Hz, $h_v = 5.5$ mm and $\phi = 6$ mm) and corrected considering both the filtering effects (present even for the best sampling configuration) and the distance to the channel bed using the values predicted by the conceptual model. Figures 1 to 5 show the experimental results of the percentages of turbulent kinetic energy, Reynolds shear stress and velocity variances in the streamwise, spanwise and vertical direction (k%, $\langle uw \rangle$%, var_x%, var_y% and var_z%, respectively) remaining in the signal after spatial and temporal averaging as a function of the dimensionless parameter F_{st}. It can be observed that the experimental data compare well with the conceptual model results. Best fit lines through the experimental and modelled data (using linearization) are also included and similar trends are observed for both data sets.

5 Summary and conclusions

This work presents an investigation into the spatial and temporal averaging (filtering) effects inherent in ADV operations on the estimates of the turbulent kinetic energy, velocity variances, and Reynolds shear stress. The averaging processes are implemented in ADV technology in order to reduce the noise level involved in acoustic measurements. The results show that filtering effects due to the ADV sampling strategy on the turbulence parameters decrease with an increase in the dimensionless distance from the bed $F_{st} = z/L_{ADV}$, where L_{ADV} has been defined as the maximum among the advective length scale ($L = U_c/f_R$), the sampling volume diameter (ϕ), and its height (h_v). The effects of the spatial and time averaging processes are most significant for values of F_{st} less than 5. Vertical velocity variance is the most affected parameter (var_z% lower than 20% for $F_{st} = 0.6$) while the Reynolds shear stress and streamwise velocity variance are less affected by filtering being higher than 65% at $F_{st} = 0.6$.

The results suggest that ADV should be operated at the maximum recording frequency f_R and minimum sampling volume height in order to obtain a value of F_{st} as large as possible. However, the user must be aware that increasing the recording frequency over $1.4U_c/\phi$ is not worth doing (Soulsby 1980), and that small sampling volumes and high recording frequencies might result in significant Doppler noise levels. Thus, the selection of the recording frequency and the sampling volume height should optimize F_{st} keeping the Doppler noise level as low as possible. In addition, since L_{ADV} has been defined as the maximum among $L = U_c/f_R$, ϕ and h_v, increasing the recording frequency f_R and decreasing the sampling volume height to get L and h_v smaller than $\phi = 6$ mm is not worth doing.

Acknowledgements

This research work was supported by the Consejo Nacional de Investigaciones Científicas y Técnicas (CONICET) of Argentina. The experiments were performed at the Laboratorio de Hidráulica of Facultad de Ingeniería y Ciencias Hídricas, Universidad Nacional del Litoral. MC acknowledges the funding of ANPCyT PICT-2010-2459, Comisión Nacional de Energía Atómica and Instituto Balseiro.

Notation

c	=	sound speed in water (m s^{-1})
dx, dy, dz	=	DNS grid sizes
F	=	Froude number (–)
F_{st}	=	dimensionless parameter (–)
f_s	=	sampling frequency (s^{-1})
f_R	=	recording frequency (s^{-1})
f_o	=	ADV transmitting frequency (s^{-1})
$\boldsymbol{G}$	=	dimensionless driving force (–)

g = gravity acceleration ($m\,s^{-2}$)
H = water depth (m)
$h(x,y,z)$ = spatial weighting function (–)
h_v = height of the sampling volume (m)
k = turbulent kinetic energy ($m^2\,s^{-2}$)
$k\%$ = percentage of the turbulent kinetic energy remaining in the signal after spatial and temporal averaging (–)
k_{ref} = turbulent kinetic energy at minimum filtering ($m^2\,s^{-2}$)
I, J, K = number of DNS cells (–)
L_{ADV} = ADV characteristic length scale (m)
L = length scale (m)
L_x, L_y, L_z = characteristic channel lengths (m)
l_x, l_y, l_z = sampling volume lengths (m)
N = number of time intervals (–)
N_x, N_y, N_z = number of nodes in the grid (–)
P = dimensionless pressure (–)
Q = flow discharge ($m^3\,s^{-1}$)
R = Reynolds number (–)
R_τ = friction Reynolds number (–)
$\boldsymbol{U}$ = dimensionless velocity vector (–)
U_x = mean streamwise flow velocity ($m\,s^{-1}$)
U_c = eddy convection velocity ($m\,s^{-1}$)
u_* = shear velocity ($m\,s^{-1}$)
(u, v, w) = dimensionless velocity components after averaging (–)
(u_x, u_y, u_z) = DNS dimensionless velocity components (–)
$\langle uw \rangle$ = Reynolds shear stress ($m^2\,s^{-2}$)
$\langle uw \rangle\%$ = percentage of Reynolds shear stress remaining in the signal after spatial and temporal averaging (–)
$\langle uw \rangle_{ref}$ = Reynolds shear stress at minimum filtering ($m^2\,s^{-2}$)
var_x = streamwise velocity variance ($m^2\,s^{-2}$)
var_y = spanwise velocity variance ($m^2\,s^{-2}$)
var_z = vertical velocity variance ($m^2\,s^{-2}$)
var_{xref} = streamwise velocity variance for minimum filtering ($m^2\,s^{-2}$)
var_{yref} = spanwise velocity variance for minimum filtering ($m^2\,s^{-2}$)
var_{zref} = vertical velocity variance for minimum filtering ($m^2\,s^{-2}$)
$var_x\%$ = percentage of streamwise velocity variance remaining in the signal after spatial and temporal averaging (–)
$var_y\%$ = percentage of spanwise velocity variance remaining in the signal after spatial and temporal averaging (–)
$var_z\%$ = percentage of vertical velocity variance remaining in the signal after spatial and temporal averaging (–)
v_b = along beam velocity ($m\,s^{-1}$)
x_c, y_c, z_c = coordinates of the sampling volume centre (m)
x, y, z = Cartesian coordinates (m)
$\Delta\varphi$ = phase shift (s^{-1})
Δt = pulse duration (s)
$\Delta x^+, \Delta y^+, \Delta z^+_{\max}, \Delta z^+_{\min}$ = grid sizes in wall units (–)
ϕ = sampling volume diameter (m)
λ = wavelength (m^{-1})
ν = kinematic viscosity ($m^2\,s^{-1}$)
ρ = fluid density ($kg\,m^{-3}$)
$\Delta\tau$ = timelag between pulses (s)
τ_w = bottom wall shear stress ($kg\,s^{-2}\,m^{-1}$)

References

Bendat, J., & Piersol, A. (2000). *Random data*. New York, USA: Wiley.

Blanckaert, K., & Lemmin, U. (2006). Means of noise reduction in acoustic turbulence measurements. *Journal of Hydraulic Research*, *44*(1), 3–17.

Cantero, M., Lee, J., Balachandar, J., & García. M. (2007). On the front velocity of gravity currents. *Journal of Fluid Mechanics*, *586*, 1–39.

Cortese, T., & Balachandar, S. (1995). High performance spectral simulation of turbulent flows inmassively parallel machines with distributed memory. *International Journal of Supercomputing Applications*, *9*(3), 187–204.

Doroudian, B., Bagherimiyab, F., & Lemmin, U. (2010). Improving the accuracy of four-receiver acoustic Doppler velocimeter (ADV) measurements in turbulent boundary layer flows. *Limnology and Oceanography Methods*, *8*, 575–591.

García, C., Cantero, M., Niño, Y., & García, M. (2005).s Turbulence measurements with acoustic Doppler velocimeters. *Journal of Hydraulic Engineering*, *131*, 1062–1073.

Goring, D., & Nikora, V. (2002). Despiking acoustic Doppler velocimeter data. *Journal of Hydraulic Engineering*, *121*(1), 117–126.

Kraus, N., Lohrmann, L., & Cabrera, R. (1994). New acoustic meter for measuring 3d laboratory flows. *Journal of Hydraulic Engineering*, *120*, 406–412.

Lhermitte, R., & Serafin, R. (1984). Pulse to pulse Doppler sonar signal processing techniques. *Journal of Atmospheric and Oceanic Tech*nology, *1*, 293–308.

Lohrmann, A., Cabrera, R., & Kraus, N. (1994). Acoustic Doppler velocimeter (ADV) for laboratory use. Proceedings of the International Conference on *Fundamentals and Advancements in Hydraulic Measurements and Experimentation*, *ASCE*, 351–365.

López, F., & Garcia, M. (2001). Mean flow structure of open-channel flow through non-emergent vegetation. *Journal of Hydraulic Engineering*, *127*, 392–402.

McLelland, S., & Nicholas, A. (2000). A new method for evaluating errors in high-frequency ADV measurements. *Hydrological Processes*, *14*, 351–366.

Miller, K., & Rochwarger, M. (1972). A covariance approach to spectral moment estimation. *IEEE Transactions on Information. Theory*, *18*, 588–596.

Nezu, I., & Nakagawa, H. (1993). *Turbulence in open-channel flows.* IAHR Monograph Series. Rotterdam, NL: Balkema.

Nikora, V., & Goring, D. (1998). ADV measurements of turbulence: Can we improve their interpretation? *Journal Hydraulic Engineering*, *124*, 630–634.

Parsheh, M., Sotiropoulos, F., & Porté-Agel, F. (2010). Estimation of power spectra of acoustic Doppler velocimetry data contaminated with intermittent spikes. *Journal of Hydraulic Engineering*, *136*, 368–378.

Precht, E., Janssen, F., & Huettel, M. (2006). Near-bottom performance of the acoustic Doppler velocimeter (ADV) – a comparative study. *Aquatic Ecology*, *40*, 481–492.

Romagnoli, M., García, C., & Lopardo, R. (2012). Signal post-processing technique and uncertainty analysis of ADV turbulence measurements on free hydraulic jumps. *Journal of Hydraulic Engineering*, *138*, 353–357.

Rusello, P. (2009). A practical primer for pulse coherent instruments. Technical Report TN-27, Nortek, USA.

SonTek (2001). ADV technical documentation. SonTek/YSI, San Diego, USA.

Soulsby, R. (1980). Selecting record length and digitization rate for near-bed turbulence measurements. *Journal of Physical Oceanography*, *10*, 208–219.

Tarrab, L., García, C., Cantero, M., & Oberg, K. (2012). Role of turbulence fluctuations on uncertainties of acoustic Doppler current profiler discharge measurements. *Water Resources Research*, *48*, 1–12.

Voulgaris, G., & Trowbridge, J. (1998). Evaluation of the acoustic Doppler velocimeter (ADV) for turbulence measurements. *Journal of Atmospheric and Oceanic Technology*, *15*(2), 272–288.

Zrnic, D. (1977). Spectral moment estimates from correlated pulse pair. *IEEE Transactions Aerospace and Electronic Systems*, *13*, 344–354.